

Observation of a new D_{sJ} meson in $B^+ \rightarrow \bar{D}^0 D^0 K^+$ decays

K. Abe,⁹ K. Abe,⁴⁹ I. Adachi,⁹ H. Aihara,⁵¹ D. Anipko,¹ K. Aoki,²⁵ T. Arakawa,³²
 K. Arinstein,¹ Y. Asano,⁵⁶ T. Aso,⁵⁵ V. Aulchenko,¹ T. Aushev,²¹ T. Aziz,⁴⁷ S. Bahinipati,⁴
 A. M. Bakich,⁴⁶ V. Balagura,¹⁵ Y. Ban,³⁷ S. Banerjee,⁴⁷ E. Barberio,²⁴ M. Barbero,⁸
 A. Bay,²¹ I. Bedny,¹ K. Belous,¹⁴ U. Bitenc,¹⁶ I. Bizjak,¹⁶ S. Blyth,²⁷ A. Bondar,¹
 A. Bozek,³⁰ M. Bračko,^{23,16} J. Brodzicka,^{9,30} T. E. Browder,⁸ M.-C. Chang,⁵⁰ P. Chang,²⁹
 Y. Chao,²⁹ A. Chen,²⁷ K.-F. Chen,²⁹ W. T. Chen,²⁷ B. G. Cheon,³ R. Chistov,¹⁵
 J. H. Choi,¹⁸ S.-K. Choi,⁷ Y. Choi,⁴⁵ Y. K. Choi,⁴⁵ A. Chuvikov,³⁹ S. Cole,⁴⁶ J. Dalseno,²⁴
 M. Danilov,¹⁵ M. Dash,⁵⁷ R. Dowd,²⁴ J. Dragic,⁹ A. Drutskoy,⁴ S. Eidelman,¹ Y. Enari,²⁵
 D. Epifanov,¹ S. Fratina,¹⁶ H. Fujii,⁹ M. Fujikawa,²⁶ N. Gabyshev,¹ A. Garmash,³⁹
 T. Gershon,⁹ A. Go,²⁷ G. Gokhroo,⁴⁷ P. Goldenzweig,⁴ B. Golob,^{22,16} A. Gorišek,¹⁶
 M. Grosse Perdekamp,^{11,40} H. Guler,⁸ H. Ha,¹⁸ J. Haba,⁹ K. Hara,²⁵ T. Hara,³⁵
 Y. Hasegawa,⁴⁴ N. C. Hastings,⁵¹ K. Hayasaka,²⁵ H. Hayashii,²⁶ M. Hazumi,⁹
 D. Heffernan,³⁵ T. Higuchi,⁹ L. Hinz,²¹ T. Hokuue,²⁵ Y. Hoshi,⁴⁹ K. Hoshina,⁵⁴ S. Hou,²⁷
 W.-S. Hou,²⁹ Y. B. Hsiung,²⁹ Y. Igarashi,⁹ T. Iijima,²⁵ K. Ikado,²⁵ A. Imoto,²⁶ K. Inami,²⁵
 A. Ishikawa,⁵¹ H. Ishino,⁵² K. Itoh,⁵¹ R. Itoh,⁹ M. Iwabuchi,⁶ M. Iwasaki,⁵¹ Y. Iwasaki,⁹
 C. Jacoby,²¹ M. Jones,⁸ H. Kakuno,⁵¹ J. H. Kang,⁵⁸ J. S. Kang,¹⁸ P. Kapusta,³⁰
 S. U. Kataoka,²⁶ N. Katayama,⁹ H. Kawai,² T. Kawasaki,³² H. R. Khan,⁵² A. Kibayashi,⁵²
 H. Kichimi,⁹ N. Kikuchi,⁵⁰ H. J. Kim,²⁰ H. O. Kim,⁴⁵ J. H. Kim,⁴⁵ S. K. Kim,⁴³
 T. H. Kim,⁵⁸ Y. J. Kim,⁶ K. Kinoshita,⁴ N. Kishimoto,²⁵ S. Korpar,^{23,16} Y. Kozakai,²⁵
 P. Križan,^{22,16} P. Krokovny,⁹ T. Kubota,²⁵ R. Kulasiri,⁴ R. Kumar,³⁶ C. C. Kuo,²⁷
 E. Kurihara,² A. Kusaka,⁵¹ A. Kuzmin,¹ Y.-J. Kwon,⁵⁸ J. S. Lange,⁵ G. Leder,¹³ J. Lee,⁴³
 S. E. Lee,⁴³ Y.-J. Lee,²⁹ T. Lesiak,³⁰ J. Li,⁸ A. Limosani,⁹ C. Y. Lin,²⁹ S.-W. Lin,²⁹
 Y. Liu,⁶ D. Liventsev,¹⁵ J. MacNaughton,¹³ G. Majumder,⁴⁷ F. Mandl,¹³ D. Marlow,³⁹
 T. Matsumoto,⁵³ A. Matyja,³⁰ S. McOnie,⁴⁶ T. Medvedeva,¹⁵ Y. Mikami,⁵⁰ W. Mitaroff,¹³
 K. Miyabayashi,²⁶ H. Miyake,³⁵ H. Miyata,³² Y. Miyazaki,²⁵ R. Mizuk,¹⁵ D. Mohapatra,⁵⁷
 G. R. Moloney,²⁴ T. Mori,⁵² J. Mueller,³⁸ A. Murakami,⁴¹ T. Nagamine,⁵⁰ Y. Nagasaka,¹⁰
 T. Nakagawa,⁵³ Y. Nakahama,⁵¹ I. Nakamura,⁹ E. Nakano,³⁴ M. Nakao,⁹ H. Nakazawa,⁹
 Z. Natkaniec,³⁰ K. Neichi,⁴⁹ S. Nishida,⁹ K. Nishimura,⁸ O. Nitoh,⁵⁴ S. Noguchi,²⁶
 T. Nozaki,⁹ A. Ogawa,⁴⁰ S. Ogawa,⁴⁸ T. Ohshima,²⁵ T. Okabe,²⁵ S. Okuno,¹⁷ S. L. Olsen,⁸
 S. Ono,⁵² W. Ostrowicz,³⁰ H. Ozaki,⁹ P. Pakhlov,¹⁵ G. Pakhlova,¹⁵ H. Palka,³⁰
 C. W. Park,⁴⁵ H. Park,²⁰ K. S. Park,⁴⁵ N. Parslow,⁴⁶ L. S. Peak,⁴⁶ M. Pernicka,¹³
 R. Pestotnik,¹⁶ M. Peters,⁸ L. E. Piilonen,⁵⁷ A. Poluektov,¹ F. J. Ronga,⁹ N. Root,¹
 J. Rorie,⁸ M. Rozanska,³⁰ H. Sahoo,⁸ S. Saitoh,⁹ Y. Sakai,⁹ H. Sakamoto,¹⁹ H. Sakaue,³⁴
 T. R. Sarangi,⁶ N. Sato,²⁵ N. Satoyama,⁴⁴ K. Sayeed,⁴ T. Schietinger,²¹ O. Schneider,²¹
 P. Schönmeier,⁵⁰ J. Schümann,²⁸ C. Schwanda,¹³ A. J. Schwartz,⁴ R. Seidl,^{11,40} T. Seki,⁵³
 K. Senyo,²⁵ M. E. Sevier,²⁴ M. Shapkin,¹⁴ Y.-T. Shen,²⁹ H. Shibuya,⁴⁸ B. Shwartz,¹
 V. Sidorov,¹ J. B. Singh,³⁶ A. Sokolov,¹⁴ A. Somov,⁴ N. Soni,³⁶ R. Stamen,⁹ S. Stanič,³³
 M. Starič,¹⁶ H. Stoeck,⁴⁶ A. Sugiyama,⁴¹ K. Sumisawa,⁹ T. Sumiyoshi,⁵³ S. Suzuki,⁴¹
 S. Y. Suzuki,⁹ O. Tajima,⁹ N. Takada,⁴⁴ F. Takasaki,⁹ K. Tamai,⁹ N. Tamura,³²
 K. Tanabe,⁵¹ M. Tanaka,⁹ G. N. Taylor,²⁴ Y. Teramoto,³⁴ X. C. Tian,³⁷ I. Tikhomirov,¹⁵

K. Trabelsi,⁹ Y. T. Tsai,²⁹ Y. F. Tse,²⁴ T. Tsuboyama,⁹ T. Tsukamoto,⁹ K. Uchida,⁸
 Y. Uchida,⁶ S. Uehara,⁹ T. Uglov,¹⁵ K. Ueno,²⁹ Y. Unno,⁹ S. Uno,⁹ P. Urquijo,²⁴
 Y. Ushiroda,⁹ Y. Usov,¹ G. Varner,⁸ K. E. Varvell,⁴⁶ S. Villa,²¹ C. C. Wang,²⁹
 C. H. Wang,²⁸ M.-Z. Wang,²⁹ M. Watanabe,³² Y. Watanabe,⁵² J. Wicht,²¹ L. Widhalm,¹³
 J. Wiechczynski,³⁰ E. Won,¹⁸ C.-H. Wu,²⁹ Q. L. Xie,¹² B. D. Yabsley,⁴⁶ A. Yamaguchi,⁵⁰
 H. Yamamoto,⁵⁰ S. Yamamoto,⁵³ Y. Yamashita,³¹ M. Yamauchi,⁹ Heyoung Yang,⁴³
 S. Yoshino,²⁵ Y. Yuan,¹² Y. Yusa,⁵⁷ S. L. Zang,¹² C. C. Zhang,¹² J. Zhang,⁹
 L. M. Zhang,⁴² Z. P. Zhang,⁴² V. Zhilich,¹ T. Ziegler,³⁹ A. Zupanc,¹⁶ and D. Zürcher²¹

(The Belle Collaboration)

¹*Budker Institute of Nuclear Physics, Novosibirsk*

²*Chiba University, Chiba*

³*Chonnam National University, Kwangju*

⁴*University of Cincinnati, Cincinnati, Ohio 45221*

⁵*University of Frankfurt, Frankfurt*

⁶*The Graduate University for Advanced Studies, Hayama*

⁷*Gyeongsang National University, Chinju*

⁸*University of Hawaii, Honolulu, Hawaii 96822*

⁹*High Energy Accelerator Research Organization (KEK), Tsukuba*

¹⁰*Hiroshima Institute of Technology, Hiroshima*

¹¹*University of Illinois at Urbana-Champaign, Urbana, Illinois 61801*

¹²*Institute of High Energy Physics,*

Chinese Academy of Sciences, Beijing

¹³*Institute of High Energy Physics, Vienna*

¹⁴*Institute of High Energy Physics, Protvino*

¹⁵*Institute for Theoretical and Experimental Physics, Moscow*

¹⁶*J. Stefan Institute, Ljubljana*

¹⁷*Kanagawa University, Yokohama*

¹⁸*Korea University, Seoul*

¹⁹*Kyoto University, Kyoto*

²⁰*Kyungpook National University, Taegu*

²¹*Swiss Federal Institute of Technology of Lausanne, EPFL, Lausanne*

²²*University of Ljubljana, Ljubljana*

²³*University of Maribor, Maribor*

²⁴*University of Melbourne, Victoria*

²⁵*Nagoya University, Nagoya*

²⁶*Nara Women's University, Nara*

²⁷*National Central University, Chung-li*

²⁸*National United University, Miao Li*

²⁹*Department of Physics, National Taiwan University, Taipei*

³⁰*H. Niewodniczanski Institute of Nuclear Physics, Krakow*

³¹*Nippon Dental University, Niigata*

³²*Niigata University, Niigata*

³³*University of Nova Gorica, Nova Gorica*

³⁴*Osaka City University, Osaka*

³⁵*Osaka University, Osaka*

³⁶*Panjab University, Chandigarh*

- ³⁷*Peking University, Beijing*
- ³⁸*University of Pittsburgh, Pittsburgh, Pennsylvania 15260*
- ³⁹*Princeton University, Princeton, New Jersey 08544*
- ⁴⁰*RIKEN BNL Research Center, Upton, New York 11973*
- ⁴¹*Saga University, Saga*
- ⁴²*University of Science and Technology of China, Hefei*
- ⁴³*Seoul National University, Seoul*
- ⁴⁴*Shinshu University, Nagano*
- ⁴⁵*Sungkyunkwan University, Suwon*
- ⁴⁶*University of Sydney, Sydney NSW*
- ⁴⁷*Tata Institute of Fundamental Research, Bombay*
- ⁴⁸*Toho University, Funabashi*
- ⁴⁹*Tohoku Gakuin University, Tagajo*
- ⁵⁰*Tohoku University, Sendai*
- ⁵¹*Department of Physics, University of Tokyo, Tokyo*
- ⁵²*Tokyo Institute of Technology, Tokyo*
- ⁵³*Tokyo Metropolitan University, Tokyo*
- ⁵⁴*Tokyo University of Agriculture and Technology, Tokyo*
- ⁵⁵*Toyama National College of Maritime Technology, Toyama*
- ⁵⁶*University of Tsukuba, Tsukuba*
- ⁵⁷*Virginia Polytechnic Institute and State University, Blacksburg, Virginia 24061*
- ⁵⁸*Yonsei University, Seoul*

Abstract

We report the observation of a new D_{sJ} meson produced in $B^+ \rightarrow \bar{D}^0 D_{sJ} \rightarrow \bar{D}^0 D^0 K^+$. This state has a mass of $M = 2715 \pm 11_{-14}^{+11}$ MeV/c², a width $\Gamma = 115 \pm 20_{-32}^{+36}$ MeV/c² and a spin-parity 1^- . The results are based on an analysis of 449 million $B\bar{B}$ events collected at the $\Upsilon(4S)$ resonance in the Belle detector at the KEKB asymmetric energy e^+e^- collider.

PACS numbers:

At the level of quark diagrams, the decay $B \rightarrow \bar{D}DK$ proceeds dominantly via the CKM-favored $\bar{b} \rightarrow \bar{c}W^+ \rightarrow \bar{c}\bar{s}$ transition. The transition amplitudes can be categorized as either external W - or internal W -emission (color-suppressed) diagrams. The decay $B^+ \rightarrow \bar{D}^0 D^0 K^+$ [1] can proceed through both types of diagrams, with the naive expectation that the internal W contribution to the branching fraction is suppressed relative to that of the external W by a factor of nine. B -meson decays to three-body $\bar{D}DK$ final states are a promising area for searches for new $c\bar{s}$ states as well as of some $c\bar{c}$ states lying above $D^0\bar{D}^0$ threshold. Since the externally emitted W produces $1^+, 1^-, 0^-$ states, $c\bar{s}$ mesons with these quantum numbers should be copiously produced. The unexpected discoveries of the $D_{sJ}(2317)$ and $D_{sJ}(2457)$ mesons show that our understanding of the $c\bar{s}$ spectroscopy might be incomplete. Experimental data on $c\bar{c}$ states with decay channels open to $D^{(*)}\bar{D}^{(*)}$ are scarce.

The decays $B \rightarrow \bar{D}DK$ have been previously studied with a small data sample by ALEPH [2]. Recently a comprehensive study was performed by BaBar [3]. In this letter we report the first study of the Dalitz plot of $B^+ \rightarrow \bar{D}^0 D^0 K^+$ decay.

The study is performed using data collected with the Belle detector at the KEKB asymmetric-energy e^+e^- (3.5 on 8 GeV) collider [4], operating at the $\Upsilon(4S)$ resonance ($\sqrt{s} = 10.58$ GeV) with a peak luminosity that exceeds 1.6×10^{34} cm $^{-2}$ s $^{-1}$. The data sample corresponds to the integrated luminosity of 414 fb $^{-1}$ and contains 449 million $B\bar{B}$ pairs.

The Belle detector is a large-solid-angle magnetic spectrometer that consists of a silicon vertex detector, a 50-layer central drift chamber (CDC), an array of aerogel threshold Čerenkov counters (ACC), a barrel-like arrangement of time-of-flight scintillation counters (TOF), and an electromagnetic calorimeter comprised of CsI(Tl) crystals (ECL) located inside a super-conducting solenoid coil that provides a 1.5 T magnetic field. An iron flux-return located outside of the coil is instrumented to detect K_L^0 mesons and to identify muons. The detector is described in detail elsewhere [5].

We select charged tracks that originate from the interaction region by requiring $|dr| < 0.4$ cm and $|dz| < 5$ cm, where dr and dz are the distances of closest approach to the interaction point in the plane perpendicular to the beam and along the beam axis, respectively. Charged particles are identified by using combined information from the TOF, ACC and dE/dx measurements in the CDC. Requirements on the particle identification variable are imposed that identify a charge kaon with 90% efficiency at $< 10\%$ $\pi \rightarrow K$ miss-identification probability and a charged pion with $\approx 100\%$ efficiency at $< 10\%$ $K \rightarrow \pi$ miss-identification probability. Any track that is positively identified as an electron is rejected.

Candidate $K_S^0 \rightarrow \pi^+\pi^-$ decays are identified by a displaced secondary vertex, a two-pion momentum vector that is consistent with a K_S^0 originating from the interaction point and by the invariant mass selection $|M_{\pi^+\pi^-} - m_{K_S^0}| < 15$ MeV/ c^2 . Candidate π^0 mesons are identified as pairs of ECL-identified photons, each with a minimum energy of 50 MeV, that have an invariant mass within ± 15 MeV/ c^2 of the π^0 mass.

D^0 mesons are reconstructed in the $K^-\pi^+$, $K^-\pi^+\pi^+\pi^-$, $K^-\pi^+\pi^0$, $K_S^0\pi^+\pi^-$ and K^-K^+ decay modes. We preselect D candidates using a signal window ± 30 MeV/ c^2 around the nominal D meson mass for decay modes, except for $D^0 \rightarrow K^-\pi^+\pi^0$ decays, where a larger ± 50 MeV/ c^2 signal window is used. Mass- and vertex-constrained fits are applied to all D meson candidates to improve their momentum resolution.

We retain events that have a kaon candidate and at least two candidate D^0 mesons, with allowed flavor combination and with the D^0 momenta in the $\Upsilon(4S)$ rest frame ('cms')

below the kinematical limit for $B^+ \rightarrow \bar{D}^0 D^0 K^+$. To suppress the continuum background ($e^+e^- \rightarrow q\bar{q}, q = u, d, s, c$) we require the ratio of the second to the zeroth Fox-Wolfram moments [6] to be less than 0.3. Momenta of the secondaries from a B meson candidate decay are refitted to a common vertex with an interaction point constraint that takes into account the B meson decay length.

The B meson candidates are identified by their cms energy difference, $\Delta E = \sum_i E_i - E_{\text{beam}}$, and their beam constrained mass, $M_{\text{bc}} = \sqrt{E_{\text{beam}}^2 - (\sum_i \vec{p}_i)^2}$, where $E_{\text{beam}} = \sqrt{s}/2$ is the beam energy in the cms and \vec{p}_i and E_i are the three-momenta and energies of the B candidate's decay products. For the subsequent analysis we select B candidates with $M_{\text{bc}} > 5.2 \text{ GeV}/c^2$ and $-0.4 \text{ GeV} < \Delta E < 0.3 \text{ GeV}$. Exclusively reconstructed $B^+ \rightarrow \bar{D}^0 D^0 K^+$ signal events have M_{bc} distributions that peak at the nominal B -meson mass; the ΔE distributions peak near zero.

We employ a discriminator (likelihood ratio) based on the D^0 meson signal significance to select the unique B candidate in the event, defined as: $\mathcal{LR}(M_D) = \frac{S(M_D)}{S(M_D)+B(M_D)}$, where S and B are the signal and the background probabilities respectively. This discriminator is determined from the data, for each D^0 decay mode separately, using a sample enriched in $B \rightarrow \bar{D}DK$ decays. For events with multiple $B \rightarrow \bar{D}DK$ candidates, the product $\mathcal{LR}_B = \mathcal{LR}(M_{\bar{D}}) \times \mathcal{LR}(M_D)$ is calculated and the candidate with the largest $\mathcal{LR}(B)$ is accepted. The solution with larger kaon identification likelihood $\mathcal{L}(K)$ is chosen if multiple kaon candidates are found accompanying the accepted $\bar{D}^0 D^0$ combination.

The \mathcal{LR}_B discriminator is also used to suppress combinatoric backgrounds to $B^+ \rightarrow \bar{D}^0 D^0 K^+$ and to enhance the signal purity.

The ΔE and M_{bc} distributions for the $B^+ \rightarrow \bar{D}^0 D^0 K^+$ decay candidates, selected with $\mathcal{LR}_B > 0.01$ requirement, are shown in Fig. 1. The ΔE distribution is shown for events

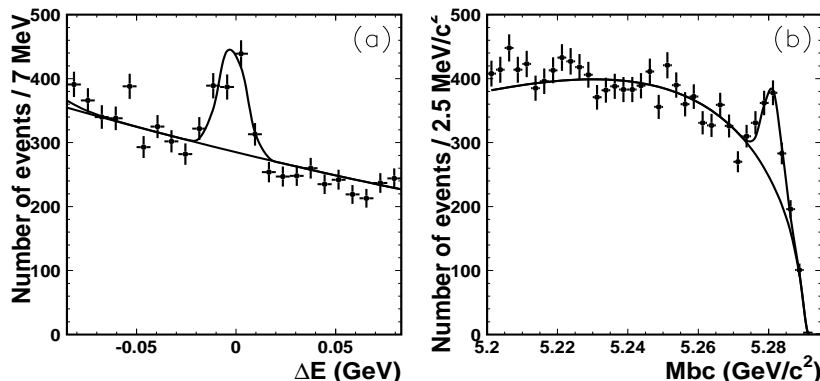


FIG. 1: ΔE (a) and M_{bc} (b) distributions for $B^+ \rightarrow \bar{D}^0 D^0 K^+$.

with $|M_{\text{bc}} - m_B| < 3\sigma_{M_{\text{bc}}}$ ($\sigma_{M_{\text{bc}}} = 2.7 \text{ MeV}/c^2$), where m_B is the nominal B meson mass and the M_{bc} distribution is shown for events with $|\Delta E| < 3\sigma_{\Delta E}$ ($\sigma_{\Delta E} = 6.6 \text{ MeV}$).

From a study of the M_{bc} and ΔE background distributions in large MC samples of generic $B\bar{B}$ and $q\bar{q}$ events, we find that the background level in the data is well explained by the MC simulations and no peaking component is seen in either distribution. Using events where one or both D^0 candidates are from the D^0 -mass sidebands, we verify with the data that there is no significant peaking background.

To extract the signal yield, we perform extended unbinned maximum-likelihood fits simultaneously to ΔE and M_{bc} . The probability density functions (PDFs) for the M_{bc} and

ΔE signals are Gaussians. The background PDF for M_{bc} is represented by a phenomenological function [7] with a phase-space-like behaviour near the kinematic boundary; the ΔE background is parameterized by a second-order polynomial. The likelihood function is maximized with free parameters for the signal yield, the Gaussian means and widths, and four parameters that describe shapes of the background distributions.

From the fit, we obtain a signal yield of $N_{sig} = 399 \pm 40$ events with a signal-to-background ratio of $S/B \simeq 0.3$. The results of the fit are superimposed on the ΔE and M_{bc} projections shown in Fig. 1. We determine the branching fraction from the relation

$$\mathcal{B}(B^+ \rightarrow \bar{D}^0 D^0 K^+) = \frac{N_{sig}}{N_{B^+B^-} \sum_{ij} \epsilon_{ij} \mathcal{B}(\bar{D} \rightarrow i) \mathcal{B}(D \rightarrow j)}, \quad (1)$$

where ϵ_{ij} are efficiencies for the i and j D subchannels and for $N_{B^+B^-}$; we assume $N_{B^+B^-} = N_{B^0\bar{B}^0}$. The efficiencies are determined by MC using a phase-space decay model. The sum in the denominator of Eq.(1) amounts to 6.8×10^{-4} .

We obtain $\mathcal{B}(B^+ \rightarrow \bar{D}^0 D^0 K^+) = (13.1 \pm 1.3_{-2.7}^{+1.7}) \times 10^{-4}$, where the first error is statistical and the second is systematic. The latter includes contributions due to uncertainties in the efficiency determination (tracking and particle identification efficiency, data-MC differences in $\Delta E, M_{bc}$ signal shapes), the \mathcal{LR}_B selection, the background parameterization, the MC model used in the efficiency calculation, the intermediate $D \rightarrow i$ branching fractions and $N_{B^+B^-}$.

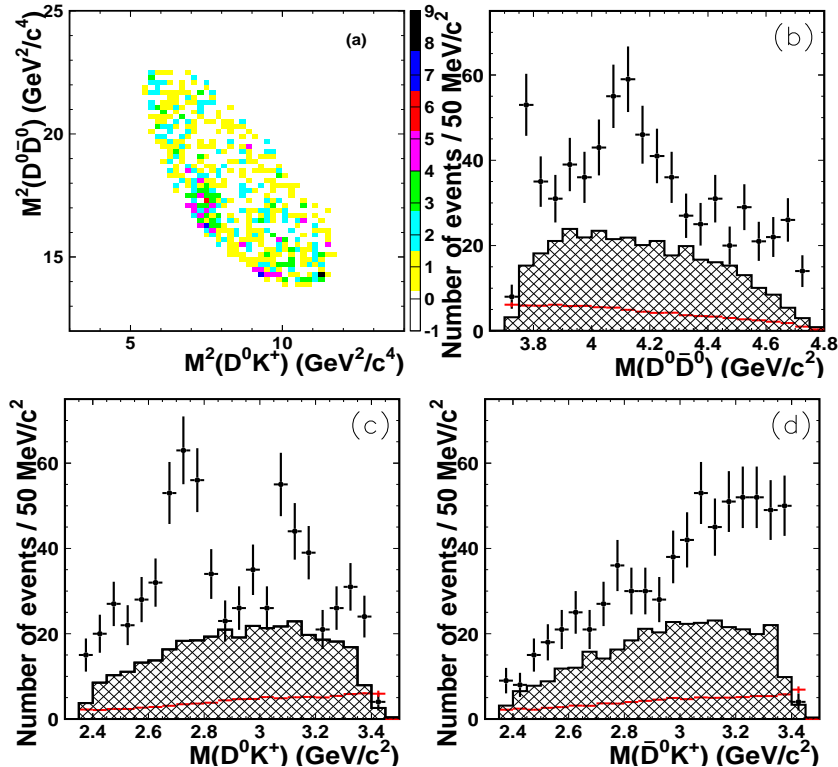


FIG. 2: Dalitz plot (a) and projections for $B^+ \rightarrow \bar{D}^0 D^0 K^+$ in 1.5σ $\Delta E - M_{bc}$ signal region: $M(D^0 \bar{D}^0)$ (b), $M(D^0 K^+)$ (c), $M(\bar{D}^0 K^+)$ (d). Hatched histograms represent background, red curves show the efficiency variation (vertical scale in %).

The Dalitz plot $M^2(D^0 \bar{D}^0)$ vs $M^2(D^0 K^+)$ for events from a signal region defined by the ellipse $(\Delta E/1.5\sigma_{\Delta E})^2 + ((M_{bc} - m_B)/1.5\sigma_{M_{bc}})^2 < 1$ is shown in Fig. 2(a). The three,

two-body invariant mass distributions are shown in Figs. 2(b)-(d). The hatched histograms represent the background distributions obtained for events from an elliptical strip surrounding the ΔE , M_{bc} signal region that extends from $6\sigma_{\Delta E}, \sigma_{M_{bc}}$ to $10\sigma_{\Delta E}, \sigma_{M_{bc}}$. The background distributions are normalized to the number of background events under the signal peaks ($\pm 1.5\sigma$) as determined from the combined ΔE and M_{bc} fit. The data shown are not efficiency corrected. The variation of efficiency as a function of invariant mass is shown in Figs. 2(b)-(d) as a continuous curve.

A pronounced feature of the Dalitz plot is the accumulation of events in the region $16 \text{ GeV}^2/c^4 < M^2(D^0\bar{D}^0) < 18 \text{ GeV}^2/c^4$ and $7 \text{ GeV}^2/c^4 < M^2(D^0K^+) < 8 \text{ GeV}^2/c^4$, possibly the overlap of a horizontal band that could be due to the $\psi(4160)$ and a vertical band that cannot be attributed to any known $c\bar{s}$ state. A horizontal band at $M^2(D^0\bar{D}^0) \simeq 14.2 \text{ GeV}^2/c^4$ corresponds to the $\psi(3770)$ production.

We employ simultaneous fits to the ΔE and M_{bc} distributions for events from each $50 \text{ MeV}/c^2$ mass bin of the Dalitz plot projection to obtain background-subtracted invariant mass distributions. In these fits the widths and positions of the Gaussians describing the signal are fixed at the values obtained for the total signal sample, while the signal yield and the background PDF's parameters are free parameters. The obtained signal yields are shown in Fig. 4 as points with error bars.

The $\psi(3770)$ signal is studied with finer, $20 \text{ MeV}/c^2$ mass bins (Fig. 3(a)). The peak is fitted in the region $M(D^0\bar{D}^0) < 4 \text{ GeV}/c^2$ with a Breit-Wigner (BW) plus a threshold function to describe a nonresonant component. The $\psi(3770)$ signal yield is 68 ± 15 events with a peak mass of $3777 \pm 3 \text{ MeV}/c^2$, and a width of $27 \pm 9 \text{ MeV}/c^2$, in agreement with the PDG averages.

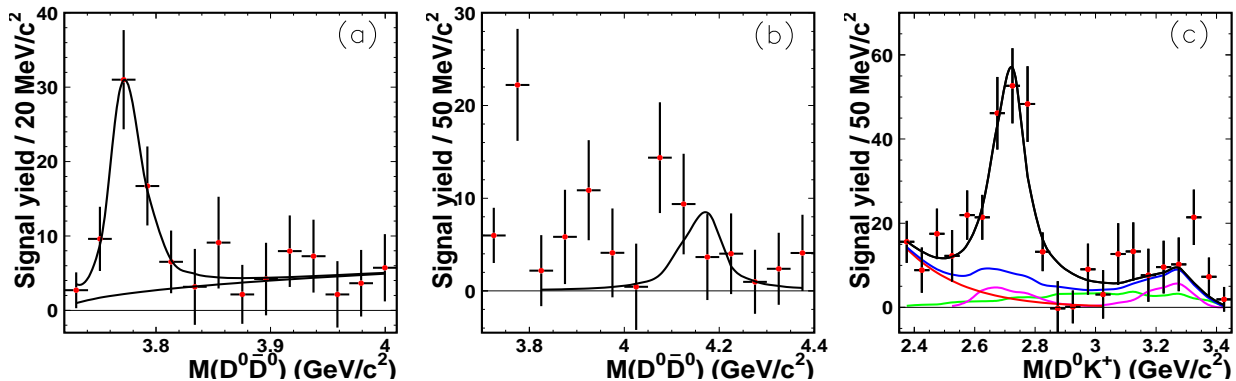


FIG. 3: Background-subtracted mass distributions: (a) $\psi(3770)$ signal, (b) $M(D^0\bar{D}^0)$ for $\cos\theta_{hel} > 0$ (c) $M(D^0K^+)$ for $M(D^0\bar{D}^0) > 3.85 \text{ GeV}/c^2$. Solid curves denote fit results described in the text. The lower curve in (a) shows phase-space component, coloured curves in (c): purple - the $\psi(4160)$ reflection, green: phase-space, red: threshold component and navy-blue: the sum of the three components.

The background-subtracted $M(D^0\bar{D}^0)$ spectrum (Fig. 3(b)), for events satisfying $\cos\theta_{hel} > 0$, where θ_{hel} is the helicity angle between the D^0 momentum vector and the boost direction to the $D^0\bar{D}^0$ rest frame, is used to estimate the possible $\psi(4160)$ contribution to the enhancement at $M(D^0K^+) \simeq 2.7 \text{ GeV}/c^2$. The distribution for $M(D^0\bar{D}^0) > 3.8 \text{ GeV}/c^2$ is fitted with a BW with mass and width fixed at the nominal $\psi(4160)$ values ($M = 4160$, $\Gamma = 80 \text{ MeV}/c^2$ [8]), yielding 24 ± 11 signal events. We use these $\psi(4160)$ parameters to

estimate the number of $\psi(4160)$ events in the backward helicity-angle hemisphere, in the region $M(D^0K^+) < 2.9 \text{ GeV}/c^2$.

Figure 3(c) shows the background-subtracted $M(D^0K^+)$ distribution for events with $M(D^0\bar{D}^0) > 3.85 \text{ GeV}/c^2$. This requirement removes the $\psi(3770)$ reflection at high $M(D^0K^+)$. The predicted $\psi(4160)$ reflection is indicated in the figure by the purple curve. The $\psi(4160)$ reflection agrees well with the data in the high mass $M(D^0K^+)$ region but does not explain the large peak at $M(D^0K^+) \simeq 2.7 \text{ GeV}/c^2$. We parameterize the observed excess of events with a BW and fit the $M(D^0K^+)$ spectrum (Fig. 3(c)) with the ansatz of a new resonance, the $\psi(4160)$ reflection shape and a phase-space component as determined by MC simulations. The free parameters in the fit are the resonance yield, mass and width, and the phase-space component normalization. The fit has an acceptable overall χ^2 but is unable to reproduce the events near the low-mass threshold seen in Fig. 3(c). We used several phenomenological parameterizations (polynomials, another BW, an exponential) of the threshold enhancement into the fit to determine its influence on the BW parameters of the $2.7 \text{ GeV}/c^2$ peak. The exponential form $a \times \exp[-\alpha M^2(D^0K^+)]$ gives a good description of the mass spectrum, while adding only two free parameters. From this fit we obtain for this new resonance, which we further denote as the $D_{sJ}^+(2700)$, a signal yield of 182 ± 30 events, mass of $M = 2715 \pm 11 \text{ MeV}/c^2$ and width of $\Gamma = 115 \pm 20 \text{ MeV}/c^2$. The threshold and the phase-space components from the fits are 58 ± 38 and 47 ± 26 events, respectively. The fit results are depicted in Figs. 4(a)-(c) as histograms overlaid on the measured mass spectra.

The resonance parameters and product branching fractions are summarized in Table I. The $\psi(4160)$ yield is not statistically significant, and therefore a 90% C.L. upper limit is also quoted. The \mathcal{B} 's of the threshold and the phase-space components are $(1.9 \pm 1.2_{-1.1}^{+1.0}) \times 10^{-4}$ and $(1.5 \pm 0.8_{-1.6}^{+0.2}) \times 10^{-4}$ (the first errors are statistical, the second are systematic) which correspond to the 90% C.L. upper limits of 4.9×10^{-4} and 3.0×10^{-4} , respectively. The systematic errors on the product branching fractions and the resonance parameters include contributions from the efficiency variation over the Dalitz plot, uncertainties in the yields of the $\psi(4160)$ reflection (including recent measurements of the $\psi(4160)$ parameters [9]), the threshold parameterization, sensitivities of parameters to the fit range and parameterization, uncertainties in the \mathcal{LR}_B selection, as well as due to neglected interference effects. The systematics due to the latter are determined from MC simulations of Dalitz plot densities with and without interference of coherent amplitudes. Here an isobar formalism was used, with each contributing resonance parameterized by the BW form. The resonance parameters from Table I and the threshold enhancement parameters are used to determine the amplitudes. The effects of interference of the $\psi(3770)$ with other states are found small and are neglected in the simulations. Events generated with maximal constructive and destructive interferences between the amplitudes, were passed through a complete detector simulation and analysed ignoring interference effects. The differences between the obtained resonance parameters and the input values are taken as their systematic errors.

We study background-subtracted $\psi(3770)$ and $D_{sJ}^+(2700)$ helicity angle distributions by selecting the respective invariant mass in the resonance region and obtaining signal yields in bins of $\cos\theta_{hel}$ from simultaneous fits to ΔE and M_{bc} . Spin-parity hypotheses for the resonances are tested by performing binned χ^2 fits to the obtained angular distributions corrected with efficiency weights. The $J = 1$ hypothesis describes the $\psi(3770)$ distribution well ($\chi^2/ndf = 3.6/5$), $J = 1$ is favoured for the $D_{sJ}^+(2700)$ ($\chi^2/ndf = 7/5$); the $J = 0$ ($185/5$) and $J = 2$ ($250/5$) assignments can be rejected.

TABLE I: Branching fractions of quasi-two-body components

R	$D_{sJ}^+(2700)$	$\psi(3770)$	$\psi(4160)$
N_{sig}	182 ± 30	68 ± 15	43 ± 20
$M(\text{MeV}/c^2)$	$2715 \pm 11_{-14}^{+11}$	$3777 \pm 3 \pm 4$	4160(fixed)
$\Gamma(\text{MeV}/c^2)$	$115 \pm 20_{-32}^{+36}$	$27 \pm 9 \pm 5$	80(fixed)
$\mathcal{B}[B^+ \rightarrow RK^+(\bar{D}^0 R)] \times$ $\mathcal{B}[R \rightarrow \bar{D}^0 D^0(D^0 K^+)]$ [10^{-4}](or 90% C.L.)	7.2 $\pm 1.2_{-2.9}^{+1.0}$	1.5 $\pm 0.3_{-0.3}^{+0.2}$	1.1 $\pm 0.5_{-0.2}^{+0.5}$ (< 2.4)

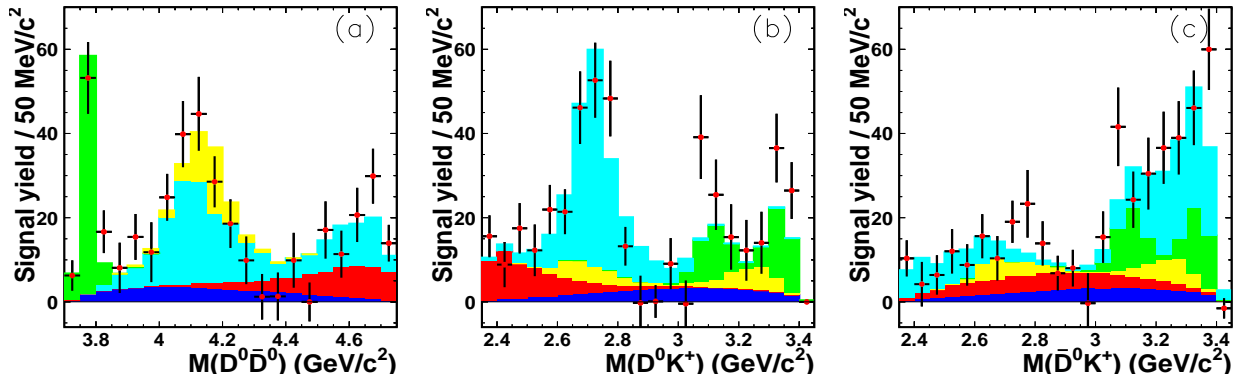


FIG. 4: $B^+ \rightarrow \bar{D}^0 D^0 K^+$ signal yield vs $M(D^0 \bar{D}^0)$ (a), $M(D^0 K^+)$ (b), and $M(\bar{D}^0 K^+)$ (c). Histograms denote the contributions from: $D_{sJ}^+(2700)$ (blue), $\psi(3770)$ (green), $\psi(4160)$ (yellow), threshold (red) and phase-space components (navy blue). Histograms are superimposed additively.

The $M(D^0 K^+)$ distribution of Fig. 2(c) in $10 \text{ MeV}/c^2$ is used to search for the $D_{sJ}(2573)$ contribution. We include this state in the fit using the BW formula with the parameters from [8], and obtain $N_{\text{sig}}(D_{sJ}(2573)) = 7.7 \pm 5.7$, which corresponds to the 90% C.L. upper limit of $\mathcal{B}(B^+ \rightarrow \bar{D}^0 D_{sJ}(2573)) \times \mathcal{B}(D_{sJ}(2573) \rightarrow D^0 K^+) < 0.7 \times 10^{-4}$.

In summary, from a study of the Dalitz plot we find that the decay $B^+ \rightarrow \bar{D}^0 D^0 K^+$ proceeds dominantly via quasi-two-body channels: $B^+ \rightarrow \bar{D}^0 D_{sJ}^+(2700)$ and $B^+ \rightarrow \psi(3770) K^+$, where $D_{sJ}^+(2700)$ is a previously unobserved resonance in the $D^0 K^+$ system with a mass $M = 2715 \pm 11_{-14}^{+11} \text{ MeV}/c^2$, width $\Gamma = 115 \pm 20_{-32}^{+36} \text{ MeV}/c^2$ and $J^P = 1^-$. The observed rate for $\psi(3770)$ production confirms our previous observation [10].

Based on its observed decay channel, we interpret the $D_{sJ}^+(2700)$ resonance as a $c\bar{s}$ meson. Potential model calculations [11] predict a $c\bar{s}$ radially excited 2^3S_1 state with mass $M = 2720 \text{ MeV}/c^2$. From chiral symmetry considerations [12] a 1^+-1^- doublet of states has been predicted. If the 1^+ state is identified as the $D_{sJ}(2536)$, the mass predicted for the 1^- state is $M = 2721 \pm 10 \text{ MeV}/c^2$. Additional measurements of the meson properties are needed to distinguish between these two interpretations.

We thank the KEKB group for the excellent operation of the accelerator, the KEK cryogenics group for the efficient operation of the solenoid, and the KEK computer group and the National Institute of Informatics for valuable computing and Super-SINET network support. We acknowledge support from the Ministry of Education, Culture, Sports, Science, and Technology of Japan and the Japan Society for the Promotion of Science; the Australian Research Council and the Australian Department of Education, Science and Training; the

National Science Foundation of China and the Knowledge Innovation Program of the Chinese Academy of Sciences under contract No. 10575109 and IHEP-U-503; the Department of Science and Technology of India; the BK21 program of the Ministry of Education of Korea, the CHEP SRC program and Basic Research program (grant No. R01-2005-000-10089-0) of the Korea Science and Engineering Foundation, and the Pure Basic Research Group program of the Korea Research Foundation; the Polish State Committee for Scientific Research; the Ministry of Science and Technology of the Russian Federation; the Slovenian Research Agency; the Swiss National Science Foundation; the National Science Council and the Ministry of Education of Taiwan; and the U.S. Department of Energy.

-
- [1] Throughout this paper, the inclusion of the charge conjugate mode decay is implied.
 - [2] R. Barate *et al.* (ALEPH Collaboration), *Eur.Phys.J. C* **4**, 387 (1998).
 - [3] B. Aubert *et al.* (BABAR Collaboration), *Phys. Rev. D* **68**, 092001 (2003).
 - [4] S. Kurokawa and E. Kikutani, *Nucl. Instr. and Meth. A* **499**, 1 (2003), and other papers included in this volume.
 - [5] A. Abashian *et al.* (Belle Collaboration), *Nucl. Instr. and Meth. A* **479**, 117 (2002).
 - [6] G. Fox, S. Wolfram, *Phys. Rev. Lett.* **41**, 278 (1990).
 - [7] H. Albrecht *et al.* (ARGUS Collaboration), *Phys. Lett. B* **299**, 304 (1989).
 - [8] S. Eidelman *et al.*, *Phys. Lett. B* **592**, 1 (2004).
 - [9] A. Osterfeld *et al.* (Crystal Ball Collaboration), SLAC-PUB-4160 (1986);
J. Z. Bai *et al.* (BES Collaboration), *Phys. Rev. Lett.* **88**, 101802 (2002).
 - [10] R. Chistov *et al.* (Belle Collaboration), *Phys. Rev. Lett.* **93**, 051803 (2004).
 - [11] S. Godfrey, N. Isgur, *Phys. Rev. D* **32**, 189 (1985).
 - [12] Maciej A. Nowak, Mannque Rho, Ismail Zahed, *Acta Phys.Polon. B* **35**, 2377 (2004).